A Highly Porous Graphitic-N Rich Carbon Stabilized Copper Nanocatalysts for Efficient Ethanol Dehydrogenation

8 authors, including:

Qing-Nan Wang
Dalian University of Technology
5 PUBLICATIONS **74** CITATIONS

Wen-Cui Li
Dalian University of Technology
127 PUBLICATIONS **6,356** CITATIONS

Mingshu Chen
Xiamen University
93 PUBLICATIONS **4,940** CITATIONS

An-Hui Lu
Dalian University of Technology
183 PUBLICATIONS **14,333** CITATIONS

Some of the authors of this publication are also working on these related projects:

SHINERS View project

mining engineering View project

A Highly Porous Carbon Support Rich in Graphitic-N Stabilizes Copper Nanocatalysts for Efficient Ethanol Dehydrogenation

Peng Zhang,[a] Qing-Nan Wang,[a] Xia Yang,[b] Dongqi Wang,[b] Wen-Cui Li,[a] Yanping Zheng,[c] Mingshu Chen,[c] and An-Hui Lu*[a]

The dehydrogenation of bioethanol to acetaldehyde and hydrogen is a sustainable process, owing to the atom-economical transformation and easy separation of the products. However, oxide-supported Cu catalysts show a low selectivity to acetaldehyde because of considerable side reactions caused by their oxygen-rich surfaces. A conventional carbon-supported Cu catalyst shows high selectivity, but is quickly deactivated owing to the migration and agglomeration of copper particles. Here, we have produced a highly porous nitrogen-rich carbon support that contains 6.2 wt % N and can nicely disperse and sta-bilize Cu nanoparticles ($\sim$ 6.3 nm). If used for ethanol dehydrogenation, approximately 98 % selectivity to acetaldehyde has been achieved, with excellent anti-agglomeration ability for as long as 500 min. X-ray photoelectron spectroscopy (XPS) data prove that electrons transfer to the Cu particles from the N sites. Theoretical calculations further show that nitrogen sites enhance the adsorption of Cu_{20} clusters and can stabilize them against coalescence and that graphitic-N sites (approximately 40 % of total N content) are the most significant.

Introduction

The production of chemicals and fuels from renewable biomass and its derivatives provides a viable route to alleviate our strong dependence on diminishing fossil fuel supplies.[1] Even though the price of fossil fuel has decreased over the last few years, it represents a non-renewable resource. Alternative sustainable options are expected to be developed as long-term energy solutions. Ethanol is particularly attractive because of its easy synthesis by biomass fermentation, and its anticipated increased availability and reduced cost.[2] Ethanol can be converted into acetaldehyde and hydrogen through a direct dehydrogenation protocol, usually named the dehydrogenation of ethanol to acetaldehyde process (DHEA).[3] This process is more promising than oxidation dehydrogenation of ethanol, which produces CH_3COOH, CO_2, CH_4, and other byproducts.[4–7] Compared with the current industrial Wacker process, which in-volves the use of $PdCl_2$ and $CuCl_2$ as catalysts in strong acidic and corrosive solutions,[8] the DHEA process may become an important alternative for the production of acetaldehyde.[9] Acetaldehyde is an important bulk intermediate in the production of other chemicals[10] and the hydrogen byproduct can be further used in hydrogenation reactions or to provide energy for fuel cells.[11]

For this endothermic ($\Delta H = +52.5 \text{ kJ mol}^{-1}$), non-oxidative, direct dehydrogenation of ethanol, copper-based catalysts appear to be most suitable.[12] Mesoporous silica-supported copper catalysts perform particularly well and the ethanol conversion can reach 85 % with a selectivity of 73 % towards acetaldehyde at 260 °C.[13] The existence of Si−O−M bonds, formed between the active metal (M, here Cu) and -OH groups on the silica surface, was identified as the key for maintaining copper stability.[14] However, the Si−OH group can also catalyze side reactions, such as the cleavage of C−O bonds, leading to ethanol dehydration[15] and the condensation or ketonization reactions of acetaldehyde to produce C3 and C4 compounds. This significantly decreases the selectivity to acetaldehyde.[16] Such intrinsic problems can also be observed if Al_2O_3, ZrO_2, or ZnO are used as catalyst support because of the presence of a large number of hydroxyl, acidic, and/or basic sites on the catalyst surface.[17]

Porous carbons, with a relatively inert surface, excellent chemical and thermal stability, and well-developed porosity,[18] have been proposed as supports to improve the acetaldehyde selectivity in ethanol dehydrogenation at high conversion rates. Indeed, copper supported on a mesoporous carbon catalyst showed excellent selectivity for the DHEA reaction.[9] How-ever, owing to the intrinsically weak interaction between

[a] P. Zhang, Q.-N. Wang, Prof. W.-C. Li, Prof. A.-H. Lu
State Key Laboratory of Fine Chemicals, School of Chemical Engineering
Dalian University of Technology
Dalian 116024 (P.R. China)
E-mail: anhuilu@dlut.edu.cn

[b] Prof. X. Yang, Prof. D. Wang
Multidisciplinary Initiative Center
Institute of High Energy Physics, Chinese Academy of Sciences
Beijing 100049 (P.R. China)

[c] Dr. Y. Zheng, Prof. M. Chen
State Key Laboratory of Physical Chemistry of Solid Surfaces, National
Engineering Laboratory for Green Chemical Productions of Alcohols,
Ethers and Esters, Department of Chemistry, College of Chemistry and
Chemical Engineering
Xiamen University
Xiamen 361005 (P.R. China)

Supporting information for this article can be found under:
http://dx.doi.org/10.1002/cctc.201601373.

copper and carbon surfaces and the low Tammann temperature of copper ($T_{tam} \approx 405\,°C$),[19] the copper particles on the carbon tend to coalescence and are easily deactivated. Hence, the use of only a physical confinement effect[20] on the porous support[21] is often insufficient to prevent this. Chemically active surfaces that can stabilize the copper particles are required, but they unavoidably cause side reactions. Thus, the real dilemma or challenge is to prepare a porous carbon support that can both physically and chemically stabilize copper nanoparticles against agglomeration while minimizing the side reactions by exposing only inactive surfaces to the targeted reactions.

As a response to the aforementioned issues, we have designed a polyacrylonitrile-based porous carbon (PPC) with open macropores, thin skeletal struts, and a particularly high content of graphitic-N (approximately 40% of the total nitrogen content). Ex situ X-ray photoelectron spectroscopy (XPS) and density functional theory (DFT) calculations together prove that the graphitic-N sites play a significant role in stabilizing the active copper phase under the reaction conditions. The intrinsic open macropore structure is favorable for fast diffusion kinetics, resulting in a short residence time of the products on the active sites,[22] thus further suppressing secondary reactions. Such a carbon-supported copper catalyst exhibits excellent stability and approximately 98% selectivity to acetaldehyde in the DHEA reaction. This selectivity is substantially higher than that of previously reported SiO_2, Al_2O_3, and other oxide-supported copper catalysts.

Results and Discussion

The PPC supports were prepared by using acrylonitrile as the carbon and nitrogen source and a small amount of graphene oxide (GO) through a series of polymerization, oxidative stabilization, carbonization, and activation processes. The oxidative stabilization step is necessary to obtain cross-linked polyacrylonitrile chains with a ladder structure.[23] The drastic shrinkage of polyacrylonitrile during the carbonization caused great tension stress, which bent the GO sheets to form macropores. Finally, a macro-microporous structure can be obtained with the help of CO_2 activation by which micropores in the pore walls were created without destroying the macroporous framework. The morphology and structure evolution of the PPC is shown in Figure S1 (in the Supporting Information).

As seen in Figure 1a and b, the PPC support shows highly developed macropores formed by interconnected curved, thin carbon walls. TEM observation (Figure 1c) indicates that the PPC has an amorphous structure with few graphitic layers formed during the carbonization of polyacrylonitrile.[24] The Raman spectrum of PPC (Figure 1d) indicates the coexistence of amorphous and graphitic carbon based on the D band (1350 cm^{-1}), G band (1590 cm^{-1}), and 2D region (2400–3250 cm^{-1}).[25] Elemental and XPS analyses were used to determine the element contents. As shown in Table 1, the nitrogen content evaluated from the elemental analysis is 6.2 wt% and from XPS is 4.7 wt%, showing that the number of surface nitrogen groups is less than that in the bulk material.
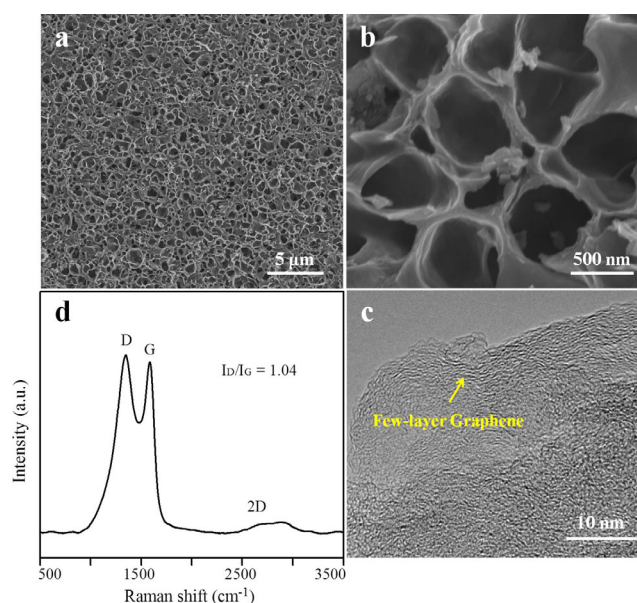

Figure 1. (a, b) Field emission (FE)-SEM images, (c) high-resolution (HR)-TEM image, and (d) Raman spectrum of PPC.

Table 1. Elemental analysis of the carbon samples.

Supports	Elemental analysis[a] [wt%]				XPS[b] [wt%]			% of total N 1s[c] [wt%]				
	C	N	O	H	C	N	O	N1	N2	N3	N4	N5
PPC	77.1	6.2	15.1	1.6	89.0	4.7	6.4	24.7	12.8	40.7	11.6	10.2
NGC	75.3	6.5	16.4	1.8	86.8	5.0	8.2	22.5	13.0	43.1	11.3	10.1

[a] The C, N, O, and H contents were directly measured by elemental analysis. [b] Weight percentage of C, N, and O elements obtained from XPS analysis. [c] N1, pyridinic-N; N2, pyrrolic-N; N3, graphitic-N; N4, N-oxides; and N5, chemisorbed N.

SEM examination of PPC at different stages of its preparation (Figure S1 in the Supporting Information) confirmed that the structure was formed during carbonization and essentially maintained during activation. It is worth pointing out that GO shows such a strong shape-directing effect. However, without GO, the prepared sample (named NGC) shows a solid skeleton (Figure S2a in the Supporting Information), but a similar crystalline state and the same microporous features and surface nitrogen content as PPC (Figures S2b–d in the Supporting Information and Table 1). The XRD patterns of both supports are shown in Figure S3 (in the Supporting Information).

After Cu nanoparticles were dispersed on the surface of PCC and NGC, the catalytic performance of Cu/PPC and Cu/NGC for DHEA was investigated at 260°C under atmospheric pressure. As a control sample, commercial microporous carbon (CMC) with similar porous features to NGC but without nitrogen dopants was used to prepare a copper catalyst (Cu/CMC).[26] Its Raman spectrum and XRD pattern are shown in Figures S3 and S4 (in the Supporting Information). The nitrogen sorption isotherms (Figure S5 in the Supporting Information) of all three materials are typical type I isotherms, indicating the presence of abundant micropores in the carbon walls. CMC (991 m^2 g^{-1})

⟰⟰ These are not the final page numbers!

has a higher surface area than both PPC (787 m^{2}g^{-1}) and NGC (916 m^{2}g^{-1}). The catalysis results for the three samples are shown in Figures 2, S4, and S5 (in the Supporting Information), and their structural parameters are summarized in Table 2. The
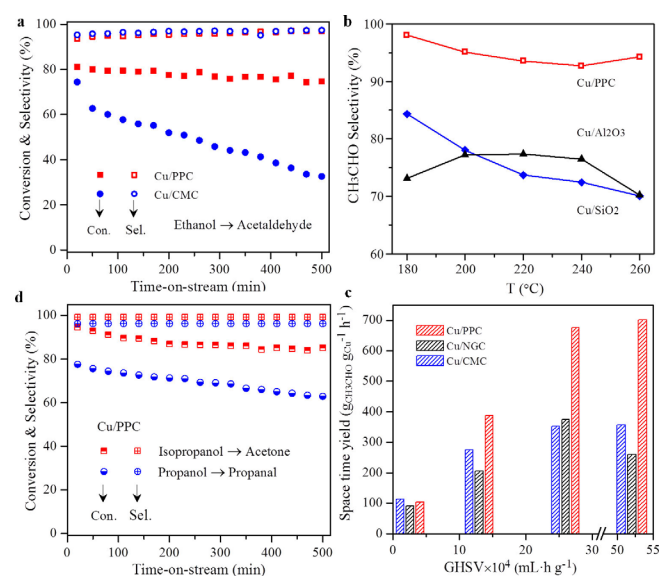

Figure 2. (a) Ethanol dehydrogenation activities over Cu/PPC and Cu/CMC with time at 260 °C. (b) CH$_3$CHO selectivity over Cu/PPC, Cu/SiO$_2$, and Cu/Al$_2$O$_3$ catalysts as a function of reaction temperature. (c) Dependence of the space time yield of CH$_3$CHO on the gas hourly space velocity (GHSV) over Cu/PPC, Cu/NGC, and Cu/CMC at 260 °C. (d) Dehydrogenation activities of propanol (at 170 °C) and isopropanol (at 260 °C) over the Cu/PPC catalyst.

Table 2. Structure parameters of the catalysts.

Catalysts	Cu [wt%]	Dispersion of Cu [%][a]	Cu surface [m$_{Cu}^2$ g$_{Cu}^{-1}$][a]	Particle size [nm] TEM	Particle size [nm] N$_2$O[b]
Cu/PPC	10	18.3	123.8	6.3	6.3
Cu/NGC	10	18.8	127.5	6.5	6.1
Cu/CMC	10	15.4	104.1	8.6	7.5

[a] Dispersion and surface of copper were determined by N$_2$O surface oxidation and H$_2$ temperature-programmed reduction (TPR) titration. [b] Cu particle size is obtained from the dispersion data.

ethanol conversion increased as the reaction temperature was increased, especially at temperatures above 200 °C (Figure S6 a in the Supporting Information), which complies with the endothermic feature of this reaction.[27] The ethanol conversion over Cu/PPC and Cu/NGC remains about 80 % after a 500 min test but this value dramatically dropped from 76 % to 32 % for the Cu/CMC catalyst (Figure 2 a). Moreover, the selectivity to acetaldehyde over all of these catalysts is higher than 95 % during this stability test. Compared with Cu/PPC, SiO$_2$- and Al$_2$O$_3$-supported copper catalysts show selectivities to acetaldehyde lower than 77 % (Figures 2 b and S6 b in the Supporting Information), and further analysis (Figures S6 c and d in the Supporting Information) indicates the advantage of the chemically inert nature of carbon materials in minimizing the secondary reactions of acetaldehyde. The gas hourly space velocity

(GHSV) effect was further investigated to reveal the advantages of such a structure with thin skeletal struts and open macropores. As shown in Figure 2 c, if an ultra-high GHSV of 520 000 mL h g^{-1} was used, a very high space time yield (i.e., grams of CH$_3$CHO formed per gram of Cu per hour) of about 700 was achieved if Cu/PPC was used as catalyst. The improvement in the space time yield for Cu/PPC was substantially larger than those with the Cu/CMC and Cu/NGC catalysts if the GHSV was increased from 26 000 to 520 000 mL h g^{-1}. This trend shows that the hierarchical macro- and microporous structure of PPC benefits mass transfer and diffusion, which helps avoid secondary reactions from the point of view of dynamics.

To evaluate the versatility of this Cu/PPC catalyst in alcohol dehydrogenation, propanol and isopropanol were also used as reactants, and high catalytic performance was observed, as shown in Figure 2 d.

The TEM images in Figure 3 a–c and Figure S8 a–b (in the Supporting Information) show that almost identical Cu particles are homogenously distributed on the surface of the PPC and NGC supports for both fresh and spent catalysts. Statistical analysis shows that more than 80 % of the particles for fresh and spent Cu/PPC fall in the size range of 6.3–6.7 nm. These values are substantially smaller than those supported on carbon nanofibers,[28] and graphene,[29] which are approximately 20 nm and 25 nm, respectively. For the fresh Cu/PPC, the high-resolution TEM image, in Figure 3 b, shows that the Cu particle has a d-spacing of about 2.087 Å, which corresponds to the Cu (111) plane. This is in agreement with the XRD pattern (Figure 3 d), which mainly exhibits a diffraction peak of a (111) facet. In contrast, the Cu particle size of Cu/CMC increased noticeably from 8.6 nm to about 20 nm after the reaction (Figure S8 c and d in the Supporting Information), which is responsible for the dramatic deactivation. Clearly, the differ-
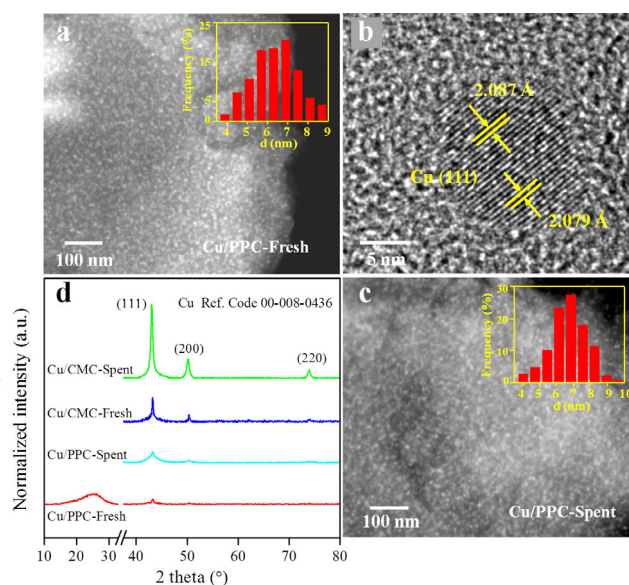

Figure 3. (a, b) TEM images of the fresh Cu/PPC catalysts. (c) High angle annular dark field (HAADF)-STEM image of the spent Cu/PPC catalysts after ethanol dehydrogenation for 500 min. (d) XRD patterns of the catalysts.

These are not the final page numbers! ↗↗

ence between Cu/PPC and Cu/CMC in their catalytic activity is attributed to the large number of nitrogen dopants, which provide more anchoring sites for the stabilization of Cu nanoparticles in the former system.

To get a definitive answer about which of these N species has a crucial effect on the stabilization of copper on the PPC surface, XPS of PPC and Cu/PPC after H_2 reduction was performed. As seen in Figure 4a, the fitting of the high-resolution N 1s peak gave the following results: N1 (pyridinic-N, 398.16–
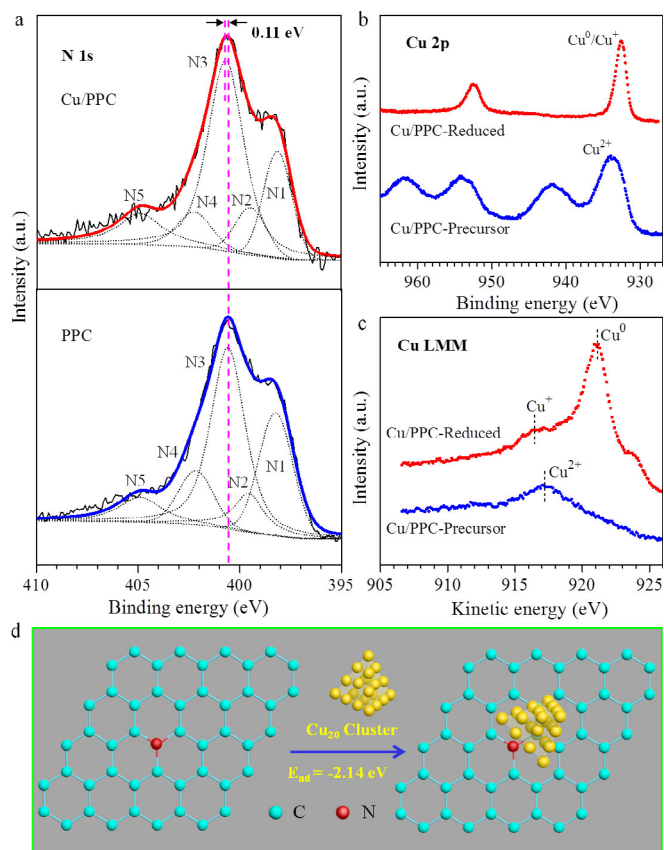

Figure 4. (a) N 1s spectra of PPC and Cu/PPC obtained after hydrogen reduction: N1, pyridinic-N; N2, pyrrolic-N; N3, graphitic-N; N4, *N*-oxides; and N5, chemisorbed N. (b) Cu 2p and (c) Cu LMM X-ray-excited Auger electron spectroscopy (XAES) spectra of the Cu/PPC catalyst obtained before and after hydrogen reduction. (d) The adsorption energy of a Cu_{20} cluster on graphitic-N-doped graphene.

398.18 eV), N2 (pyrrolic-N, 399.53–399.54 eV), N3 (graphitic-N, 400.56–400.67 eV), N4 (*N*-oxides, 402.25–402.23 eV), and N5 (chemisorbed N, 404.90–404.93 eV),[30] and the relative contents of these functionalities are summarized in Table 1. Sample PPC includes 40% graphitic-N (N3) in total. After Cu loading, the N3 peak shifted clearly by about 0.11 eV towards higher binding energy, indicating a decrease in electron density around graphitic-N species (Table S3 in the Supporting Information). However, the shift in binding energy of other N species is negligible (Table S3 in the Supporting Information), indicating very weak electron interactions with the Cu particles. The absence of an XPS peak at 933.93 eV strongly indicates that most Cu^{2+} species have been reduced to Cu^0 or Cu^+

(932.56 eV). The kinetic energy of the Cu LMM illustrates that Cu^0 is the major component, although a small fraction of Cu^+ is formed. The asymmetric kinetic energy peak is centered at 916.45 eV for Cu^+ and 921.15 eV for Cu^0. The Cu^0 peak shows a higher kinetic energy than the commonly reported one at around 919 eV,[31] indicating that the electron density around the Cu is enriched. The remaining oxygenic groups around the Cu particles after the reduction step (Figure S9 in the Supporting Information) may account for the formation of the small amount of Cu^+ species.

To reveal the strength of the electronic interaction between these N sites and Cu, DFT calculations were performed to obtain the adsorption energies of a copper cluster (Cu_{20}) to the pristine and three N-doped graphene models: pyridinic-N (N1), pyrrolic-N (N2), and graphitic-N (N3). The results indicate that the N atom is highly negatively charged, regardless of doping type (Figure S10 in the Supporting Information). The atomic charge is not uniformly distributed in the Cu_{20} cluster, and the atoms in the center of the face carry a positive charge of approximately 0.03 e, whereas the atoms at the other positions carry negative charges. This gives a better fit for the adsorption of the Cu_{20} cluster to the N-doped graphenes than to pristine graphene. On adsorption of this Cu cluster on N3-type graphene, the charge of N varies from −0.43 to −0.42 e. This is in line with the XPS results as shown in Figure 4a and Table S3 (in the Supporting Information). Indeed, the calculated adsorption energies of the Cu_{20} cluster to the four types of surfaces (pristine, pyridinic, pyrrolic, and graphitic-N graphenes) are −0.62, −0.82, −0.98, and −2.14 eV, respectively (Figure 4d and Table S4 in the Supporting Information). This suggests that the adsorption of copper clusters on graphene is thermodynamically favorable, and that the adsorption energy to the one doped with graphitic-N is the strongest.

Conclusions

We have prepared a highly porous, N-doped carbon containing a large number of graphitic-N sites, which can act as supports for anchoring and stabilizing Cu nanoparticles during the DHEA reaction. By combining a large number of anchoring sites and enhanced mass transport, Cu/PPC manifests very superior stability and high selectivity compared with other catalysts reported so far. This study opens a new approach for the preparation of highly active and selective carbon-supported copper nanocatalysts that can catalyze the conversion of alcohol to aldehyde in atom-economical transformation.

Experimental Section

Preparation of supports and catalysts

The following materials were used as received. Ammonium persulfate (APS), copper(II) nitrate trihydrate (>99.0%), and ethanol (99.7%) were supplied by Sinopharm Chemical Reagent Co., Ltd. Acrylonitrile was purchased from Gracia (Chengdu) Chemical Technology Co., Ltd. Commercial microporous carbon (CMC) was supplied by PICA, France. The graphene oxide (GO) colloids were prepared by using a modified Hummers method, which combines

↖↖ **These are not the final page numbers!**

chemical functionalization with physical exfoliation through strong stirring or sonication of high purity graphite. By using this process, the GO sheets can be functionalized with numerous groups including carboxylic acids, hydroxyls, and epoxides, for exploitation in other reactions. The as-obtained concentrated GO was dispersed in deionized water with the aid of sonication. Before use, the concentration of the GO colloids was measured by the weight difference of an amount of GO colloids before and after drying.

Support preparation: Typically, GO colloids (30 mL, 3 mg mL^{-1}) were dispersed under sonication for 30 min (denoted solution A). Afterwards, APS (180 mg) was dissolved in deionized water (1 mL) with magnetic stirring at room temperature (RT). Then, acrylonitrile (6 g) was added to this solution and stirred for 5 min (denoted solution B). Solutions A and B were then mixed at RT and stirred for another 10 min. The obtained black homogeneous aqueous solution was then transferred into a sealed bottle and put in an oven at 70 °C. It quickly turned yellow and solidified within 15 min. This gel was then cured for an additional 7 h. The as-made polymer monolith was then dried at 50 °C followed by stabilization at 270 °C for 4 h in air and pyrolysis at 800 °C for 2 h in N$_2$. After pyrolysis, this sample was also activated in CO$_2$ at 900 °C to produce porous structures, denoted as PPC. For comparison, a pure polyacrylonitrile-based porous carbon without GO precursor was also prepared in this method, and named as NGC.

Catalyst preparation: Cu/carbon catalysts containing 10 wt% copper were prepared by incipient wetness impregnation of the carbon with a Cu(NO$_3$)$_2$·3H$_2$O aqueous solution (0.625 g mL^{-1}). After impregnation, the catalyst precursors were kept at room temperature for 30 min followed by drying at 50 °C for 12 h. Catalysts were reduced by 10 vol% H$_2$ balanced with N$_2$ at 450 °C for 2 h. For comparison, Cu/NGC and Cu/CMC were also prepared by using this method.

Computational details

All geometric optimizations were performed by using the density functional theory (DFT) method using the Perdew–Burke–Ernzerhof (PBE) functional[32] as implemented the in DmoL3 code.[33] The dispersion correction was included as suggested by Grimme et al.[33a] The d-polarization included basis set (DNP) was used for C, H, and N elements,[33] and copper (Cu) was treated by a quasi-relativistic effective core potential (ECP) together with the corresponding basis set optimized for the valence shells. Spin-polarization calculation was used. The Brillouin-zone integrations were performed by using Monkhorst–Pack grids, with (4×4×1) k-points meshes used for the (5×5) graphene cell. During the optimization, all atoms were allowed to relax until the residual forces were below 0.001 eV Å^{-1}.

Catalyst characterization

Scanning electron microscope (SEM) investigations of the samples were performed with a NOVA NanoSEM 450 instrument. Transmission electron microscopy (TEM) images of the samples were obtained with a Tecnai G220S-Twin electron microscope equipped with a cold field emission gun. The acceleration voltage was 200 kV. Nitrogen adsorption isotherms were measured with an ASAP 3000 sorption analyzer (Micromeritics). Before the measurements, the carbon samples were degassed under vacuum at 200 °C for 4 h until the pressure was below 0.05 mbar. The Brunauer–Emmett–Teller (BET) method was used to calculate the specific sur-

face area (S_{BET}). The total pore volume (V_{total}) was calculated from the amount adsorbed at a relative pressure, P/P_0 of 0.99. Elemental analysis was performed with a CHNO elemental analyzer (Vario EL III, Elementar). Raman spectra were collected with a homemade DL-2 microscopic Raman spectrometer, by using the 244 or 532 nm line of a KIMMON laser. X-ray diffraction (XRD) patterns were obtained with a Panalytical X'pert Pro Super X-ray diffractometer using CuK$_\alpha$ radiation (40 kV, 40 mA, $\lambda = 0.15418$ nm). H$_2$–N$_2$O titration was used to measure the copper dispersion and average particle size at 90 °C by using a procedure described in the literature.[34] X-ray photoelectron spectroscopy (XPS) data were obtained with a PHI 5000 Versaprobe spectrometer equipped with an AlK$_\alpha$ X-ray source. Prior to testing, the sample was in situ reduced at 450 °C for 2 h by using 10 vol% H$_2$ balanced with Ar. The binding energy was calibrated by using the C 1s peak at 284.6 eV. The obtained carbon monolith was polished to a thin carbon plate, into which the Cu precursor was impregnated.

Catalytic tests and product analysis

DHEA was performed in a fix-bed reactor under atmospheric pressure. Typically, the catalyst (100 mg) was placed in the above reactor. Before the reaction, this catalyst was pre-reduced by 10 vol% H$_2$ in N$_2$ at 450 °C for 2 h. On cooling to 100 °C, ethanol (weight hourly space velocity, WHSV = 2.4 h^{-1}) was introduced into an evaporator (100 °C) by a syringe pump and carried into the reactor by flowing nitrogen gas with a flow rate of 40 mL min^{-1} (C$_2$H$_5$OH/N$_2$ = 5:95, molar). The product line was heated at 120 °C before a cold trap, which was used to condense the liquid products. A GC7900 Gas Chromatograph (GC), fitted with a FFAP capillary column and a flame ionization detector (FID), was connected to the line between the reactor outlet and the cold trap to analyze the products in the effluent gas. After the cold trap, the dry gas was examined by a thermal conductivity detector (TCD) equipped with 5A and GDX-102 molecular sieve columns for the analysis of the gas products (e.g., C$_2$H$_4$, CH$_4$, and others). The CH$_4$ content measured by FID was used to calibrate the TCD measurement. The carbon balance of these reactions is more than 96%. For kinetic analysis, Arrhenius plots of the reaction rate over the catalysts were obtained at 453–533 K, WHSV$_{C2H5OH}$ = 190 h^{-1}, and C$_2$H$_5$OH/N$_2$ = 1:4. The isopropanol and propanol dehydrogenation reactions were measured at conditions of WHSV = 3.12 h^{-1} and N$_2$ = 40 mL min^{-1} at 170 °C and 260 °C, respectively.

Acknowledgments

[1] a) P. Gallezot, *Chem. Soc. Rev.* **2012**, *41*, 1538–1558; b) D. M. Alonso, J. Q. Bond, J. A. Dumesic, *Green Chem.* **2010**, *12*, 1493–1513; c) M. H. Tucker, A. J. Crisci, B. N. Wigington, N. Phadke, R. Alamillo, J. Zhang, S. L. Scott, J. A. Dumesic, *ACS Catal.* **2012**, *2*, 1865–1876; d) C. Angelici, B. M. Weckhuysen, P. C. A. Bruijnincx, *ChemSusChem* **2013**, *6*, 1595–1614.

[2] a) J. Sun, J. Zhu, F. Gao, C. Wang, J. Liu, C. H. Peden, Y. Wang, *J. Am. Chem. Soc.* **2011**, *133*, 11096–11099; b) J. Rass-Hansen, H. Falsig, B. Jør-

gensen, C. H. Christensen, *J. Chem. Technol. Biotechnol.* **2007**, *82*, 329–333.

[3] a) R. Prasad, *Mater. Lett.* **2005**, *59*, 3945–3949; b) V. L. Sushkevich, I. I. Ivanova, E. Taarning, *ChemCatChem* **2013**, *5*, 2367–2373.

[4] M. V. Morales, E. Asedegbega-Nieto, B. Bachiller-Baeza, A. Guerrero-Ruiz, *Carbon* **2016**, *102*, 426–436.

[5] W. H. Cassinelli, L. Martins, A. R. Passos, S. H. Pulcinelli, A. Rochet, V. Briois, C. V. Santilli, *ChemCatChem* **2015**, *7*, 1668–1677.

[6] P. Liu, E. J. M. Hensen, *J. Am. Chem. Soc.* **2013**, *135*, 14032–14035.

[7] J. Mielby, J. O. Abildstrøm, F. Wang, T. Kasama, C. Weidenthaler, S. Kegnæs, *Angew. Chem. Int. Ed.* **2014**, *53*, 12513–12516; *Angew. Chem.* **2014**, *126*, 12721–12724.

[8] J. A. Keith, P. M. Henry, *Angew. Chem. Int. Ed.* **2009**, *48*, 9038–9049; *Angew. Chem.* **2009**, *121*, 9200–9212.

[9] a) V. I. Sobolev, K. Y. Koltunov, O. A. Simakova, A.-R. Leino, D. Y. Murzin, *Appl. Catal. A* **2012**, *433*, 88–95; b) T. Takei, N. Iguchi, M. Haruta, *Catal. Surv. Asia* **2011**, *15*, 80–88.

[10] C. Caro, K. Thirunavukkarasu, M. Anilkumar, N. Shiju, G. Rothenberg, *Adv. Synth. Catal.* **2012**, *354*, 1327–1336.

[11] B. Sakintuna, F. Lamari-Darkrim, M. Hirscher, *Int. J. Hydrogen Energy* **2007**, *32*, 1121–1140.

[12] a) R. Rioux, M. Vannice, *J. Catal.* **2003**, *216*, 362–376; b) F. Wang, R. Shi, Z.-Q. Liu, P.-J. Shang, X. Pang, S. Shen, Z. Feng, C. Li, W. Shen, *ACS Catal.* **2013**, *3*, 890–894.

[13] Q.-N. Wang, L. Shi, A.-H. Lu, *ChemCatChem* **2015**, *7*, 2846–2852.

[14] J. Gong, H. Yue, Y. Zhao, S. Zhao, L. Zhao, J. Lv, S. Wang, X. Ma, *J. Am. Chem. Soc.* **2012**, *134*, 13922–13925.

[15] N. Iwasa, N. Takezawa, *Bull. Chem. Soc. Jpn.* **1991**, *64*, 2619–2623.

[16] a) S.-i. Fujita, N. Iwasa, H. Tani, W. Nomura, M. Arai, N. Takezawa, *React. Kinet. Catal. Lett.* **2001**, *73*, 367–372; b) A. G. Sato, D. P. Volanti, I. C. de Freitas, E. Longo, J. M. C. Bueno, *Catal. Commun.* **2012**, *26*, 122–126.

[17] R. Reiche, R. Thielsch, S. Oswald, K. Wetzig, *J. Electron Spectrosc. Relat. Phenom.* **1999**, *104*, 161–171.

[18] a) R. Lv, T. Cui, M. S. Jun, Q. Zhang, A. Cao, D. S. Su, Z. Zhang, S. H. Yoon, J. Miyawaki, I. Mochida, *Adv. Funct. Mater.* **2011**, *21*, 999–1006; b) D. S. Su, S. Perathoner, G. Centi, *Chem. Rev.* **2013**, *113*, 5782–5816.

[19] *Handbook of Heterogeneous Catalysis* (Eds.: G. Ertl, H. Knözinger, F. Schüth, J. Weitkamp), Wiley-VCH, Weinheim, **2008**.

[20] a) J. Lu, B. Fu, M. C. Kung, G. Xiao, J. W. Elam, H. H. Kung, P. C. Stair, *Science* **2012**, *335*, 1205–1208; b) H. N. Pham, A. E. Anderson, R. L. Johnson, T. J. Schwartz, B. J. O'Neill, P. Duan, K. J. Schmidt-Rohr, A. Dumesic, A. K. Datye, *ACS Catal.* **2015**, *5*, 4546–4555; c) H. Xiong, T. J. Schwartz, N. I. Andersen, J. A. Dumesic, A. K. Datye, *Angew. Chem. Int. Ed.* **2015**, *54*, 7939–7943; *Angew. Chem.* **2015**, *127*, 8050–8054.

[21] X. Pan, Z. Fan, W. Chen, Y. Ding, H. Luo, X. Bao, *Nat. Mater.* **2007**, *6*, 507–511.

[22] Z. Y. Jin, A. H. Lu, Y. Y. Xu, J. T. Zhang, W. C. Li, *Adv. Mater.* **2014**, *26*, 3700–3705.

[23] Y. Yao, T. Zhou, T. Yang, R. Xiang, Y. Wu, *Carbon* **2013**, *58*, 249–251.

[24] D. Zhu, C. Xu, N. Nakura, M. Matsuo, *Carbon* **2002**, *40*, 363–373.

[25] a) A. C. Ferrari, J. C. Meyer, V. Scardaci, C. Casiraghi, M. Lazzeri, F. Mauri, S. Piscanec, D. Jiang, K. S. Novoselov, S. Roth, A. K. Geim, *Phys. Rev. Lett.* **2006**, *97*, 187401; b) M. Zhou, T. Cai, F. Pu, H. Chen, Z. Wang, H. Zhang, S. Guan, *ACS Appl. Mater. Interfaces* **2013**, *5*, 3449–3455.

[26] Y. Zhang, Y. Zhang, L. Wang, H. Jiang, C. Xiong, *Ind. Eng. Chem. Res.* **2015**, *54*, 5894–5900.

[27] F.-W. Chang, H.-C. Yang, L. S. Roselin, W.-Y. Kuo, *Appl. Catal. A* **2006**, *304*, 30–39.

[28] I. Kvande, D. Chen, M. Rønning, H. J. Venvik, A. Holmen, *Catal. Today* **2005**, *100*, 391–395.

[29] A. Shaygan Nia, S. Rana, D. Döhler, X. Noirfalise, A. Belfiore, W. H. Binder, *Chem. Commun.* **2014**, *50*, 15374–15377.

[30] a) Y. Cao, H. Yu, J. Tan, F. Peng, H. Wang, J. Li, W. Zheng, N.-B. Wong, *Carbon* **2013**, *57*, 433–442; b) Z. Li, J. Liu, Z. Huang, Y. Yang, C. Xia, F. Li, *ACS Catal.* **2013**, *3*, 839–845; c) C. Weidenthaler, A.-H. Lu, W. Schmidt, F. Schüth, *Microporous Mesoporous Mater.* **2006**, *88*, 238–243; d) W. Liu, L. Zhang, W. Yan, X. Liu, X. Yang, S. Miao, W. Wang, A. Wang, T. Zhang, *Chem. Sci.* **2016**, *7*, 5758–5764.

[31] S. Sarfraz, A. T. Garcia-Esparza, A. Jedidi, L. Cavallo, K. Takanabe, *ACS Catal.* **2016**, *6*, 2842–2851.

[32] a) J. P. Perdew, K. Burke, M. Ernzerhof, *Phys. Rev. Lett.* **1996**, *77*, 3865–3868; b) J. P. Perdew, K. Burke, M. Ernzerhof, *Phys. Rev. Lett.* **1997**, *78*, 1396.

[33] a) B. Delley, *J. Chem. Phys.* **1990**, *92*, 508–517; b) B. Delley, *J. Chem. Phys.* **2000**, *113*, 7756–7764.

[34] Y. Wang, Y. Shen, Y. Zhao, J. Lv, S. Wang, X. Ma, *ACS Catal.* **2015**, *5*, 6200–6208.

↖↖ **These are not the final page numbers!**

FULL PAPERS

Killing two birds with one stone:
Copper nanoparticles can be dispersed and stabilized over highly porous carbon enriched with graphitic-N (approximately 40% of total N content), and this catalyst shows approximately 98% selectivity to product with excellent anti-agglomeration ability for as long as 500 min in ethanol dehydrogenation to acetaldehyde.
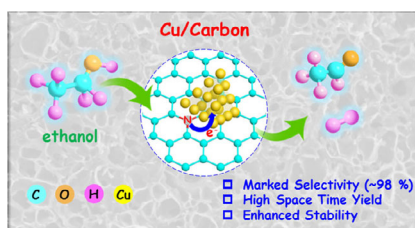
P. Zhang, Q.-N. Wang, X. Yang, D. Wang, W.-C. Li, Y. Zheng, M. Chen, A.-H. Lu*

■■ – ■■

A Highly Porous Carbon Support Rich in Graphitic-N Stabilizes Copper Nanocatalysts for Efficient Ethanol Dehydrogenation

These are not the final page numbers! ↗↗